Filling the gaps: Gaussian mixture models from noisy, truncated or incomplete samples

Peter Melchior[a], Andy D. Goulding[a]

[a]*Department of Astrophysical Sciences, Princeton University, Princeton, NJ 08544, USA*

arXiv:1611.05806v1 [astro-ph.IM] 17 Nov 2016

Abstract

We extend the common mixtures-of-Gaussians density estimation approach to account for a known sample incompleteness by simultaneous imputation from the current model. The method called `GMMis` generalizes existing Expectation-Maximization techniques for truncated data to arbitrary truncation geometries and probabilistic rejection. It can incorporate an uniform background distribution as well as independent multivariate normal measurement errors for each of the observed samples, and recovers an estimate of the error-free distribution from which both observed and unobserved samples are drawn. We compare `GMMis` to the standard Gaussian mixture model for simple test cases with different types of incompleteness, and apply it to observational data from the NASA *Chandra* X-ray telescope. The PYTHON code is capable of performing density estimation with millions of samples and thousands of model components and is released as an open-source package at `https://github.com/pmelchior/pyGMMis`.

Keywords:

1. Introduction

The Gaussian mixture model (GMM) is an important tool for many data analysis tasks, usually employed to approximate a potentially complex density distribution for which there is no known parametric form, or to perform probabilistic clustering. Its importance is reflected in the wide range of applications and the number of extensions it has received (we refer the reader to e.g. McLachlan & Peel 2000 for an overview). In this work, we will generalize the customary Expectation-Maximization (EM) algorithm to account for "incomplete" samples, i.e. a generalization of truncated samples where data from arbitrarily shaped subdomains of the feature space have a specified probability of not being reported. Also known as "sample selection bias", it constitutes a long-standing problem for robust inference of population statistics in many scientific disciplines.

Several approaches for dealing with truncated data within the context of Gaussian mixtures have been presented. Given a simple truncation boundary, one can analytically integrate the Gaussian density distribution over the unobserved subdomains (e.g. Wolynetz, 1979; Lee & Scott, 2012, and references therein). McLachlan & Jones (1988) and Cadez et al. (2002) developed a method for binned data, which requires integration of the Gaussian distribution within bins, and realized that any truncated data can be thought to belong to one extra bin, for which the moments of the GMM are already fully specified by the values in the observed bins. Provided the binning is sufficiently fine, this approach allows for arbitrarily shaped truncation boundaries at the cost of introducing, and integrating over, bins for the entire observed domain.

Our approach instead follows a proposal by Dempster et al. (1977) that an estimate of the missing data be drawn from the current model and the EM be run on the combined (observed and estimated missing) data until convergence. This approach does not require binning and provides the flexibility and computational efficiency we seek. The method we develop here is similar to multiple-imputation schemes (Rubin, 1987) for samples with missing features, and we will draw from the terminology developed in the latter context to clarify what kind of incompleteness our density-estimation method can account for.

The outline of the paper is as follows: In Section 2 we describe the EM algorithm for GMM optimization, show how it can accommodate noisy samples, and generalize it for incomplete and potentially noisy samples. We discuss several practical extensions of the algorithm in Section 3 and demonstrate the performance of the proposed algorithm on a variety of test cases in Section 4. As this work is motivated by problems in observational astronomy, we will present an example with spatially varying completeness and positional uncertainty in Section 5, and conclude in Section 6.

The method is implemented in pure PYTHON, scalable to millions of samples and thousands of GMM components, and released as an open-source package at `https://github.com/pmelchior/pyGMMis`.

2. GMM from noisy, incomplete samples

For a general mixture model over a d-dimensional feature space $\mathbb{R}^d$, the probability density function (PDF) is

$$p(\mathbf{x}\,|\,\boldsymbol{\theta}) = \sum_{k=1}^{K} \alpha_k\, p(\mathbf{x}\,|\,\theta_k), \tag{1}$$

with mixing weights that obey $\sum_k \alpha_k = 1$ and component density functions $p(\mathbf{x}\,|\,\boldsymbol{\theta}_k)$ with parameters $\boldsymbol{\theta}_k$. We will, for the sake

Email address: `peter.melchior@princeton.edu` (Peter Melchior)

of brevity, abbreviate the latter as $p_k(\mathbf{x})$. For a GMM, p_k is given by a multivariate normal distribution function,

$$p_k(\mathbf{x}) = \mathcal{N}(\mathbf{x}\,|\,\boldsymbol{\mu}_k, \boldsymbol{\Sigma}_k) \equiv \frac{\exp\left[-\frac{1}{2}(\mathbf{x}-\boldsymbol{\mu}_k)^\top \boldsymbol{\Sigma}_k^{-1}(\mathbf{x}-\boldsymbol{\mu}_k)\right]}{\sqrt{(2\pi)^d \det(\boldsymbol{\Sigma}_k)}}, \quad (2)$$

the complete set of parameters per component is thus α_k, $\boldsymbol{\mu}_k$, and $\boldsymbol{\Sigma}_k$. The associated log-likelihood for the data $\mathbf{x}_i$ with $i \in \{1, \ldots, N\}$ given fixed parameters is

$$\ln \mathcal{L} = \sum_i^N \ln \sum_k^K \alpha_k p_k(\mathbf{x}_i). \quad (3)$$

Following Bovy et al. (2011), we introduce an indicator variable

$$q_{ik} = \begin{cases} 1 & \text{if } \mathbf{x}_i \text{ is generated by component } k \\ 0 & \text{else,} \end{cases} \quad (4)$$

which allows us to rewrite Equation 3 as

$$\ln \mathcal{L} = \sum_{i,k} q_{ik} \ln\left(\alpha_k p_k(\mathbf{x}_i)\right). \quad (5)$$

2.1. Standard EM algorithm

Realizing that one can interpret q_{ik} as the probability that $\mathbf{x}_i$ is generated by component k, we can now write down the sequence of the EM algorithm, which evaluates the likelihood at fixed parameters (the E-step) and then updates the model parameters (the M-step):

$$\begin{aligned} \text{E-step:}\quad & q_{ik} \leftarrow \frac{\alpha_k p_k(\mathbf{x}_i)}{\sum_j \alpha_j p_j(\mathbf{x}_i)} \\ \text{M-step:}\quad & \alpha_k \leftarrow \frac{1}{N}\sum_i q_{ik} \equiv \frac{1}{N} q_k \\ & \boldsymbol{\mu}_k \leftarrow \frac{1}{q_k}\sum_i q_{ik}\mathbf{x}_i \\ & \boldsymbol{\Sigma}_k \leftarrow \frac{1}{q_k}\sum_i q_{ik}\left[(\boldsymbol{\mu}_k - \mathbf{x}_i)(\boldsymbol{\mu}_k - \mathbf{x}_i)^\top\right]. \end{aligned} \quad (6)$$

Dempster et al. (1977), later corrected by Wu (1983), showed that such a sequence monotonically converges to a local maximum of $\mathcal{L}$.

2.2. EM algorithm with noisy samples

Observed data often exhibit measurement uncertainties, which we assume to be additive and Gaussian:

$$\mathbf{y}_i \equiv \mathbf{x}_i + \mathbf{e}_i, \quad (7)$$

where $\mathbf{e}_i \sim \mathcal{N}(\mathbf{0}, \mathbf{S}_i)$. We want to emphasize that we do not assume that uncertainties are identical. Bovy et al. (2011) derived an extended EM algorithm that maximizes the likelihood of the noise-free density $p(\mathbf{x})$ from noisy samples $\mathbf{y}$. The key insight is that one can treat the unknown values $\mathbf{x}_i$ as parameters of the model that will be optimized themselves. With a slight simplification of the equations in Bovy et al. (2011)[1], we define $\mathbf{T}_{ik} \equiv \Sigma_k + \mathbf{S}_i$ and arrive at

$$\begin{aligned} \text{E-step:}\quad & q_{ik} \leftarrow \frac{\alpha_k p_k(\mathbf{y}_i\,|\,\boldsymbol{\mu}_k, \mathbf{T}_{ik})}{\sum_j \alpha_j p_j(\mathbf{y}_i\,|\,\boldsymbol{\mu}_j, \mathbf{T}_{ij})} \\ & \mathbf{b}_{ik} \leftarrow \boldsymbol{\mu}_k + \boldsymbol{\Sigma}_k \mathbf{T}_{ik}^{-1}(\mathbf{y}_i - \boldsymbol{\mu}_k) \\ & \mathbf{B}_{ik} \leftarrow \boldsymbol{\Sigma}_k - \boldsymbol{\Sigma}_k \mathbf{T}_{ik}^{-1}\boldsymbol{\Sigma}_k \\ \text{M-step:}\quad & \alpha_k \leftarrow \frac{1}{N}\sum_i q_{ik} \equiv \frac{1}{N} q_k \\ & \boldsymbol{\mu}_k \leftarrow \frac{1}{q_k}\sum_i q_{ik}\mathbf{b}_{ik} \\ & \boldsymbol{\Sigma}_k \leftarrow \frac{1}{q_k}\sum_i q_{ik}\left[(\boldsymbol{\mu}_k - \mathbf{b}_{ik})(\boldsymbol{\mu}_k - \mathbf{b}_{i,k})^\top + \mathbf{B}_{ik}\right]. \end{aligned} \quad (8)$$

By including measurement uncertainties in the definition of q_{ik}, the M-step is almost unchanged: the role of $\mathbf{x}_i$, which is not directly observable, is played by $\mathbf{b}_{ik}$, and the covariances get extra contributions $\mathbf{B}_{ik}$. All of those modifications vanish when $\mathbf{S}_i \to \mathbf{0}$. The resulting EM algorithm still converges monotonically to a local maximum of $\mathcal{L}$.

2.3. EM algorithm with incomplete samples

We will now proceed to generalize the EM algorithm to account for sample incompleteness, by which we mean the following: the probability of a sample $\mathbf{x}$ being observed at all is determined by an completeness function, $\Omega(\mathbf{x})$, which means that in any subdomain $\mathcal{D} \subset \mathbb{R}^d$ the density of observed samples can systematically deviate from the true density in that region. Such a situation may arise if a measurement device is incapable of recording samples from $\mathcal{D}$, so that $\Omega(\mathbf{x}) = 0\ \forall \mathbf{x} \in \mathcal{D}$. This is the typical situation of truncated samples. A softer version is given by $\Omega(\mathbf{x}) \neq 1$, which occurs when observations suffer from under- or over-reporting.[2]

One can in principle correct an observed density $p(\mathbf{x})$ by dividing with $\Omega(\mathbf{x})$, but if the inverse of the completeness is not expressible as a GMM, the corrected distribution cannot itself be described as a GMM, thus losing its convenient analytic properties. Furthermore, if in some $\mathcal{D}$ the completeness is zero, such a correction would be ill-defined. Instead, we propose to fit a GMM that can correct for incomplete sampling by iteratively imputing samples drawn from the current model in domains of reduced or zero completeness. To the best of our knowledge, this is the first time that a GMM approach has been made robust against not just truncation but the generalized form of incomplete sampling.

Before we adapt the EM algorithm to incorporate Ω, it is instructive to clarify how our concept of completeness relates to the existing terminology of "missingness" introduced by

[1] We ignore their projection matrix $\mathbf{R}_i$ as the samples in our application are either fully observed or fully missing. If needed, all relevant equations in this work can be re-derived with arbitrary sample projection matrices.

[2] Without a loss in generality, we will assume that the latter has been properly corrected, so that $\Omega(\mathbf{x}) \leq 1$, e.g. by $\Omega(\mathbf{x}) \to \Omega(\mathbf{x})/\max_{\mathbf{x}}\{\Omega(\mathbf{x})\}$. We do, however, assume that there are not false positives in the data.

Rubin (1976, see Appendix A). In short, we distinguish

$$\Omega = \begin{cases} \text{const.} & \text{missing completely at random (MCAR)} \\ \Omega(\mathbf{x}) & \text{missing at random (MAR)} \\ \Omega(\mathbf{x}, p(\mathbf{x})) & \text{missing not at random (MNAR).} \end{cases} \tag{9}$$

MCAR situations are irrelevant for density estimation as the resulting probability density function is simply a renormalized version of the true PDF. But since a density estimator necessarily obeys $\int p(x)\,dx = 1$, this normalization will automatically be removed. Thus, MCAR data yield the same density estimate, it is merely constrained by fewer samples. Under MAR, the likelihood function remains unchanged and necessary corrections to the density estimates can entirely be derived from the observed samples and the knowledge of Ω. In this situation, we can derive an exact EM algorithm to account for incomplete data. In contrast, under MNAR the likelihood function needs to be modified to incorporate the relation between the missing data and the density itself (see e.g. Schafer & Graham 2002), a generalization that goes beyond the scope of this work.

As the likelihood function under MAR is the same for the incomplete sampling case, the E-step remains unchanged and all corrections have to appear in the M-step. Lee & Scott (2012) demonstrated that the effects of simple truncation can be addressed by computing the zero-th, first, and second moments of each Gaussian component when truncated in the same way as the data, which requires the analytic integration of p_k within the observed bounds. Essentially, the update equations for $\boldsymbol{\mu}_k$ and $\boldsymbol{\Sigma}_k$ get a correction term from the difference between the current-iteration parameters and their truncated values.

As we seek the ability to employ arbitrary completeness functions, with complex spatial shapes and probabilistic rejection, the analytical integration becomes cumbersome. One could use Monte-Carlo integration instead to compute the moments under any kind of Ω, but there is an even more direct approach: creating an approximate sample of "missing" data $\mathcal{M}$, which augments the observed sample $\mathcal{O}$ to yield an estimate of how the data would be distributed with $\Omega = 1$. Effectively, we draw a sample of size oN, with scaling factor o, from the current GMM, apply rejection sampling according to Ω, and keep the rejected sample as $\mathcal{M}$ with size $N^{\mathcal{M}}$. Because of the linearity in the data, we can split both E-step and M-step into an observed and a missing sample part, so that Equation 6 becomes

$$\begin{aligned}
\text{E-step:}\quad & q_{ik} \leftarrow \frac{\alpha_k p_k(\mathbf{x}_i)}{\sum_j \alpha_j p_j(\mathbf{x}_i)} \;\forall i \in \{\mathcal{O}, \mathcal{M}\} \\
\text{M-step:}\quad & \alpha_k \leftarrow \frac{1}{N + \frac{1}{o}N^{\mathcal{M}}}\left(\sum_{i\in\mathcal{O}} q_{ik} + \frac{1}{o}\sum_{i\in\mathcal{M}} q_{ik}\right) \equiv \frac{1}{N'} q_k \\
& \boldsymbol{\mu}_k \leftarrow \frac{1}{q_k}\left(\sum_{i\in\mathcal{O}} q_{ik}\mathbf{x}_i + \frac{1}{o}\sum_{i\in\mathcal{M}} q_{ik}\mathbf{x}_i\right) \\
& \boldsymbol{\Sigma}_k \leftarrow \frac{1}{q_k}\left(\sum_{i\in\mathcal{O}} q_{ik}\left[(\boldsymbol{\mu}_k - \mathbf{x}_i)(\boldsymbol{\mu}_k - \mathbf{x}_i)^\top\right] + \right. \\
& \qquad \left. \frac{1}{o}\sum_{i\in\mathcal{M}} q_{ik}\left[(\boldsymbol{\mu}_k - \mathbf{x}_i)(\boldsymbol{\mu}_k - \mathbf{x}_i)^\top\right]\right).
\end{aligned} \tag{10}$$

This approach, called `GMMis`, in which at each iteration we draw and augment the observed data with an imputation sample, is efficient where $p(\mathbf{x})\,(1 - \Omega(\mathbf{x}))$ is large. Correction for weakly expressed components are more difficult to attain because $\mathcal{M}$ is drawn globally from the entire GMM, as opposed to from each component individually. A minor limitation is that when Ω is large for a component, the values of the $\mathcal{M}$-sums in the M-step equations are not well determined, however their impact on the result is also minor because that component is mostly observed.

In comparison with an analytic evaluation of the PDF in the unobserved domains, this approach is flexible and efficient, does not require numerical integrations, but suffers from sample variance in the correction terms because $\mathcal{M}$ has finite size. This means that the observed $\mathcal{L}$ is not guaranteed to monotonically increase, which can affect convergence criteria. One could attempt to smooth out $\mathcal{L}$ across iterations, but one can also increase the oversampling factor o when drawing $\mathcal{M}$, so that the sampled corrections become more accurate. In practice, we found $o = 1$ to often result in sample variances that are small compared to the increase of the observed likelihood until close to convergence, so that we simply terminate the EM sequence whenever $\mathcal{L}$ decreases. For sparsely sampled data, larger values of o can become necessary to stabilize the algorithm.

Besides speed and flexibility, `GMMis` retains the ability to deal with noisy samples. By adding noise to the imputation sample $\mathcal{M}$, we can evaluate q_{ik}, $\mathbf{b}_{ik}$, and $\mathbf{B}_{ik}$ for $i \in \mathcal{M}$ and modify Equation 8 analogously to Equation 10. To do so, we have to define $\mathbf{T}_{ik}$ for the missing samples, which do not have *observed* uncertainties. In some cases the positional uncertainties are known even in unobserved regions. If not, we need to make a guess of $\mathbf{S}(\mathbf{x})$ in the unobserved domain, e.g. from the mean or a smooth interpolator of the observed $\mathbf{S}_i$. We caution that not assuming errors for the $\mathcal{M}$ sample would result in too large an effective weight in the EM steps because we evaluate its likelihood in the E-step without noise while the observed sample has a broadened likelihood due to the noise. As a result, the EM algorithm would become unduly dominated by missing samples and yield density estimates that are shifted towards regions of low Ω. By the same token, we do not have to exactly match the uncertainties of $\mathcal{M}$ to those of $\mathcal{O}$ as they only ever enter in the sums of the M-step. Matching the average uncertainties for each components is therefore sufficient.

While we want to point out that artificially adding noise and applying Ω do not commute, for both cases it is sufficient to create $\mathcal{M}$ such that it completes the data with an estimate of the unobserved portion.

3. Practical considerations

3.1. Initialization

The EM algorithm only guarantees convergence to a local maximum of the likelihood. With the large number of free parameters of the GMM ($1 + d + d(d+1)/2$ for each of K components), a suitable initialization is critical. Several initialization schemes have been proposed (e.g. Biernacki et al., 2003; Blömer & Bujna, 2013). For a completely observed data set, we

adopt the simplest strategy, namely drawing the means at random from the data. In detail, given a user-defined length scale s, for each component k we draw i at random from $\{1, \ldots, N\}$ and $\Delta\mathbf{x}_i \sim \mathcal{N}(\mathbf{0}, s^2\mathbf{I})$, and set

$$\begin{aligned} \alpha_k &= 1/K \\ \boldsymbol{\mu}_k &= \mathbf{x}_i + \Delta\mathbf{x}_i \\ \boldsymbol{\Sigma}_k &= s^2\mathbf{I}, \end{aligned} \tag{11}$$

which naturally follows the distribution of the data on scales larger than s. To prevent strong initial localization, s should be chosen to exceed the typical clustering scale of the data, but small enough that multiple components do not massive overlap.

In the case of incomplete samples, we initialize the components with a previous EM run of the same data while assuming $\Omega = 1$. This leads to components that attempt to approximate the observed sample distribution, and will obviously fail if a component is entirely located in a region with $\Omega = 0$. In all other cases, we found that an initial guess based on the observed distribution much more quickly converges than the random initialization described above. To aid the exploration of the domains with $\Omega < 1$, we leave the components means unchanged but multiply the covariances by a factor > 1. If that factor is chosen too small, the EM algorithm will not be able to pick up the correction terms $\sum_{i\in\mathcal{M}} q_{ik}$ etc. in Equation 10 before re-converging to the previous, observed-sample location. In turn, if the factor is chosen too large, the convergence is slowed down. We therefore recommend a factor of $2 - 4$, i.e. increasing the linear size of each component by $50 - 100\%$, as a compromise that works well in practice.

3.2. Split-and-merge operations

With a large number of free parameters, the EM algorithm can easily get trapped in local maxima of $\mathcal{L}$. For clustered data, this behavior leads to GMM components being placed across several clusters or a single cluster being shared by multiple components. In the latter case, the weight α_k tends to zero for at least one of those components.

To improve the performance of the GMM, Ueda et al. (2000) devised criteria to decide whether a component should be merged with another or be split into two. Performing both of these operations at the same time amounts to altering three distinct components with the total number of components being conserved. We follow this approach, with two alterations we found to perform better for all cases with $d = 2, 3$ we investigated.

Ueda et al. (2000) proposed to merge the components k and l that maximize

$$J_{\mathrm{merge}}(k, l) = Q_k^\top Q_l, \tag{12}$$

with $Q_k^\top = (q_{1k}, \ldots, q_{Nk})$, i.e. the components whose posterior cluster assignment $p(k\,|\,\mathbf{x})$ are most similar across the entire data set. This works well in practice as long as there are no "empty" components, which do unfortunately arise in multimodal situations if more components are locally available than are needed to explain the data. Because $q_{ik} \to 0$ when $\alpha_k \to 0$, the merge criterion above will not seek to merge such empty components even though they are obviously excellent choices to be merged. We therefore replace $Q_k \to Q_k/\alpha_k$, which means that we seek to merge components whose $p_k(\mathbf{x})$ is most similar for the entire data set.

For the split criterion, we found that the one suggested by Ueda et al. (2000), based on the Kullback-Leibler divergence, is unduly affected by outliers and often leads to split candidates that do not improve the likelihood. Instead, we took guidance from a proposal of Zhang et al. (2003) how to best re-initialize the two new components that result from a split, namely to separate their means along the semi-major axis of the ellipsoid described by the pre-split $\boldsymbol{\Sigma}$. It thus felt natural to identify split candidates according to their largest eigenvalue λ_1 of $\boldsymbol{\Sigma}$. When searching for the component $k = \mathrm{argmax}_k\{\lambda_{k,1}\}$, we assume it is strongly elongated because it seeks to describe two clusters at once. The main failure mode of that split criterion is again related to (almost) empty components. Their parameters, in particular $\boldsymbol{\Sigma}_k$, are only poorly determined. Some of them are erroneously large and would thus be identified as split candidates, while they constitute much better merge candidates. We thus propose to identify split candidates by selecting k as the one that maximizes

$$J_{\mathrm{split}}(k) = \alpha_k \lambda_{k,1}. \tag{13}$$

While the original split criterion of Ueda et al. (2000) will seek to eliminate *any* deviation of the local density from its approximation by a Gaussian-shaped component and is therefore generally applicable, our criterion appears to perform better for identifying a prominent failure mode for unconstrained GMMs: components that merge two clusters. While this scheme may seem to result in increased fragmentation by penalizing the largest components, we have not found that to be that case because the split is only accepted if it leads to an overall increase in the likelihood. Following Zhang et al. (2003), we then replace the means of two newly split components l and m as $\boldsymbol{\mu}_{l,m} = \boldsymbol{\mu}_k \pm \frac{1}{2} EV_1(\boldsymbol{\Sigma}_k)$, i.e. along the primary eigenvector of the covariance matrix.

When dealing with incomplete data, we have not found split-and-merge operations to be problematic. They are most useful when enabled during the initialization run as described in Section 3.1, which will then not be plagued by strong failure modes of the EM algorithm. As a result, the imputation samples $\mathcal{M}$ will be more reliable, and the full algorithm will converge faster than without split-and-merge operations.

3.3. Minimum covariance regularization

One problem of the objective function $\mathcal{L}$ is that it becomes unbounded if $\boldsymbol{\mu}_k = \mathbf{y}_i$ for any k and i because $\boldsymbol{\Sigma}_k \to \mathbf{0}$. Bovy et al. (2011) presented a Bayesian regularization scheme to set a lower bound for every component volume. In its simplest version it assumes the form of a d-dimensional sphere with variance w, which modifies the last update equation in Equation 8 according to

$$\boldsymbol{\Sigma}_k \leftarrow \frac{1}{q_k + 1}\left[\sum_i q_{ik}\left[(\boldsymbol{\mu}_k - \mathbf{b}_{ik})(\boldsymbol{\mu}_k - \mathbf{b}_{i,k})^\top + \mathbf{B}_{ik}\right] + w\mathbf{I}\right]. \tag{14}$$

In principle, the value of w is entirely arbitrary, but we choose to provide a more intuitive setting and associate it with a minimum scale ω in feature space, below which the model does not possess explanatory power, i.e. we want $\det(\Sigma_k) \geq \omega^{2d}$. For a constant regularization term, we need to adopt a typical value of q_k, for which we use its mean over all components, $\bar{q}_k = \frac{N}{K}$. We can thus set $w = \omega^2(\frac{N}{K} + 1)$. This choice does not provide an exact lower bound for each component as we determine the regularization term from the average value of q_k, which leads to stronger regularization for components with small α_k. We consider this an advantage in noisy situations, where the parameters of weakly expressed components can be hard to determine.

We note, however, that the form of the regularization in Equation 14 prefers features in the data to be of approximately equal size, otherwise the penalty term can dominate for small features while being ineffective for large features.

3.4. Fitting for an uniform background

In many situations, observed data comprise anomalous samples that appear unrelated to the features of interest and rather originate from a more uniform "background" distribution. One solution within the context of GMMs would be to add another component with very large variance and to fit for its amplitude only. We prefer to introduce a truly uniform distribution over the relevant region $\mathcal{D}$ of feature space, whose intensity ν may or may not be known. This gives rise to a two-level mixture model (Frühwirth-Schnatter, 2006, their section 7.2.4) that extends Equation 1:

$$\begin{aligned} p(\mathbf{x}\,|\,\boldsymbol{\theta}) &= (1-\nu)\sum_{k=1}^{K}\alpha_k\, p(\mathbf{x}\,|\,\theta_k) + \nu p_{\mathrm{bg}}(\mathbf{x}) \\ \text{with } p_{\mathrm{bg}}(\mathbf{x}) &= \left[\int_{\mathcal{D}} d\mathbf{x}\right]^{-1} = \text{const.} \end{aligned} \tag{15}$$

The top-level mixture with weight ν requires another indicator variable Q to denote if a sample $\mathbf{x}_i$ belongs to the "signal", and is thus meant to be fit by the GMM, or to the background. Analogous to q_{ik} in Equation 6 it can be determined from

$$Q_i \leftarrow \frac{\nu p_{\mathrm{bg}}}{\nu p_{\mathrm{bg}} + (1-\nu)\sum_k \alpha_k p_k(\mathbf{x}_i)} \tag{16}$$

and has an equivalent M-step to determine the amplitude,

$$\nu \leftarrow \frac{1}{N}\sum_i Q_i. \tag{17}$$

The key for the second-level GMM fit is to exclude samples with $Q_i > u_i \sim \mathcal{U}(0,1)$, i.e. those whose current posterior favors the association with the background model. With this restricted subset the M-step can proceed as in Equation 6.

One could think that sample incompleteness does not affect the inference of the background component because any information how $\Omega(\mathbf{x})$ acts on samples drawn from p_{bg} is already entirely contained in $\Omega(\mathbf{x})$ itself.[3] The problem with this notion is that we do not know the relative amplitudes of signal and background in the unobserved regions, which will vary because the signal does. For consistent results, we therefore create the imputation sample $\mathcal{M}$ by drawing from the GMM *and* the background model according to the current-iteration value of ν, and proceed as in Section 2.3.

We caution that the introduction of a background component leads to additional uncertainties and a higher-dimensional parameter space. In particular, during the first iterations of the EM algorithm, the parameters of the GMM often only provide rather poor description of the data, so that many samples will have higher probability under the background model, resulting in few samples left to fit for the GMM parameters in the next iteration. This failure mode highlights the importance of a suitable initialization when working with a background model, especially when its intensity becomes dominant. To this end, we found in our tests that the k-means initialization from Blömer & Bujna (2013, their Algorithm 1) performed more robustly than the random initialization of Equation 11.

3.5. Averaging estimators

Even with well-chosen initial values and split-and-merge operations, any single GMM will get trapped in local maxima of the likelihood. We therefore advocate, for two reasons, to average several GMMs fit to the same data, a technique also known as ensemble learning.

First, ensemble estimators typically outperform even the best single estimator. In particular, Smyth & Wolpert (1999) built an improved estimator by employing the "stacking" method proposed by Wolpert (1992), which uses the cross-validation result to determine non-negative weights for each model (see also Breiman, 1996). In the context of GMMs, it is useful to realize that a mixture of mixture models is still a mixture model, therefore no conceptual changes have to be made when evaluating the estimator.

Second, stacked GMMs reduce the need to determine the optimal number of components K. The main concern when determining K is that if set too high, the resulting GMM overfits the data, following spurious features that increase the variance in the prediction, while if set too low, the model does not capture essential features of the data, leading to a large prediction bias. As this topic has been extensively discussed elsewhere, we will not address it here. We do note, however, that stacking exhibits better trade-offs between bias and variance than single-model selection or uniform averaging, rendering stacked GMM particularly robust against overfitting (Smyth & Wolpert, 1999). Even more so, combining GMMs with different K, or different minimal covariance limits w (cf. Section 3.3), can provide a natural framework to describe data with a variety of spatial scales.

A decision if and how single-run GMMs are to be averaged will depend on the characteristics of the data at hand. In this work, we will only use single-run results to allow the reader to evaluate the performance of `GMMis` rather than that of the averaging scheme.

[3] The presence of a non-vanishing background intensity can therefore in principle be used to estimate $\Omega(\mathbf{x})$. However, for this work we require Ω to be known a priori.

3.6. Uncertainty and coverage analysis

With several runs on the same data we can also inspect the variance between predicted densities from each run. This serves as a direct estimate of the reliability of a single or an averaged estimator, and is particularly important in regions with $\Omega < 1$.

In cases of incomplete sampling, the proposed approach can obviously only work within some finite range around the observed points, and that range is set by the volume of the components used to describe the data. In other words, the GMM will have no predictive power in regions that are separated from the observed samples by larger distances than those that can be covered by the available components.

We seek to determine the "coverage" of the feature space $\mathbb{R}^d$ by the GMM and construct such an estimate as follows: We draw a sample of test positions uniformly from a hypercube that contains all observed samples $\mathbf{x}_i$, apply rejection sampling according to Ω, and keep the ones that remain (in contrast to those that define the missing sample $\mathcal{M}$ for Equation 10) as randomized observable sample $\mathcal{R}$. We now define a new GMM and a PDF p_c, whose components means are given by $\mathcal{R}$ but their amplitudes and covariances are drawn at random from a previously optimized GMM. We define the coverage at a test positions $\mathbf{x}^t$ as the ratio $c = p_c(\mathbf{x}^t)/p_c(\mathbf{x}^n)$, where $\mathbf{x}^n = \mathrm{argmin}_{\mathbf{x}\in\mathcal{R}}\|\mathbf{x}-\mathbf{x}^t\|$, i.e. the nearest neighbor of $\mathbf{x}^t$ in $\mathcal{R}$. The coverage is therefore the fraction of the density the original GMM could have extended from the observed sample to the test point $\mathbf{x}^t$. By construction, $c = 0$ when $\|\mathbf{x}^n - \mathbf{x}^t\|$ exceeds the largest eigenvalue of all $\mathbf{\Sigma}_k$.

4. Experiments

4.1. A toy example

We first perform a simple test with no model misspecification, i.e. we draw the original sample from a GMM with $K = 3$. In Figure 1, we show that sample as red circles. We then add a noticeable amount of Gaussian noise (blue contours) and impose a purely geometric $\Omega(\mathbf{x})$, whose boundaries are given by a box and a circle (dotted curves), resulting in the test sample (blue squares). With this test case we demonstrate how the EM algorithm reacts to the presence of both noise and a non-trivial completeness. The standard EM algorithm (top-center panel) does what one needed to expect, namely to described the observed sample as is. It clearly prefers the region inside of the boundaries and thereby misestimates amplitudes, locations, and covariances of the components affected by Ω. It also ignores the presence of noise, leading to somewhat inflated covariances.

Once the selection through Ω is considered (top right panel), `GMMis` recovers component centers and amplitudes much better (seen prominently by the shape of the top-right and the bottom-left components), however the covariances remain inflated as the presence noise is not corrected for. In the bottom-left panel, we use the full algorithm, i.e. the noise deconvolution of Equation 8 applied to Equation 10, resulting in the highest likelihood of the three variants, with just $\Delta \ln \mathcal{L} = -0.151$ compared to red sample drawn from the true underlying PDF. We can also see that all components are substantially compactified, a visual confirmation that the noise broadening has been taken into account.

By running the full algorithm (with Ω and noise treatment) ten times, we can investigate the spread associated with the given data set under the admittedly restrictive assumption of a GMM with $K = 3$. The bottom-center panel of Figure 1, whose contours have the same stretch as those of the previous panels, shows that there are considerable differences between runs, mostly associated with the Ω-boundaries. Also, the components from different runs emphasize the importance of different apparent sub-clusters. This behavior is caused by the added noise, which obscures the presence of small-scale features. As we attempt to infer the noise-free PDF from noisy samples, the models will amplify small-scale density fluctuations. Because of such spurious sub-clusters or, more generally, local minima of the likelihood, we advocate the use of more sophisticated averaging schemes, as outlined in Section 3.5.

We also inspect the estimated coverage of the features space by the adopted model (bottom-right pane of Figure 1). The contour levels are logarithmically spaced and clearly show that most of the area inside the box is entirely covered, with the exception of a minor reduction within the circle. Outside of the box, the coverage drops quickly within a length scale set by the largest component, so that PDF outside of the shown region would not be recoverable.

4.2. Sample size and noise level

In addition, we run a similar test setup as in Figure 1, using the same clusters but only a box-shaped boundary of Ω, and vary N and the noise level σ. The results are shown in the left panel of Figure 2. Unsurprisingly, increasing the sample size N always improves fidelity of the inferred PDF estimate and can in most cases offset the effects of measurement noise. If the scatter grows large compared to the size of the clusters (whose effective width corresponds to 1.45, 1.15, and 0.57, respectively), even large sample sizes do not fully recover the underlying PDF, confirming the intuitive notion that information is actually lost in such a case.

This intuition is confirmed by the results shown in the right panel of Figure 2, where we vary the observed fraction at fixed $N = 1000$. We do this by shrinking the linear size of the box in Figure 1 so as to maintain a MAR situation. Only discarding samples at random would correspond to MCAR and therefore not strongly affect the recovery of the PDF: the GMM would only notice the sparsity of the resulting sample. Instead, in the chosen setup components eventually leave the observed or even the coverage area of some very small boxes. For instance, the top-left component is entirely unobservable around $N^O/N \approx 0.3$. While it becomes obvious that a reduced observed fraction has much stronger influence on $\mathcal{L}$ than the noise level, at large σ the recovery of the PDF does not reach the fidelity of lower noise data even when it is fully observed.

4.3. Limits of applicability

We want to investigate, in a more difficult, highly multimodal situation, how strongly incomplete the sampling can be for the proposed method to still yield reasonable density estimates. We therefore set up a new test case in which we place

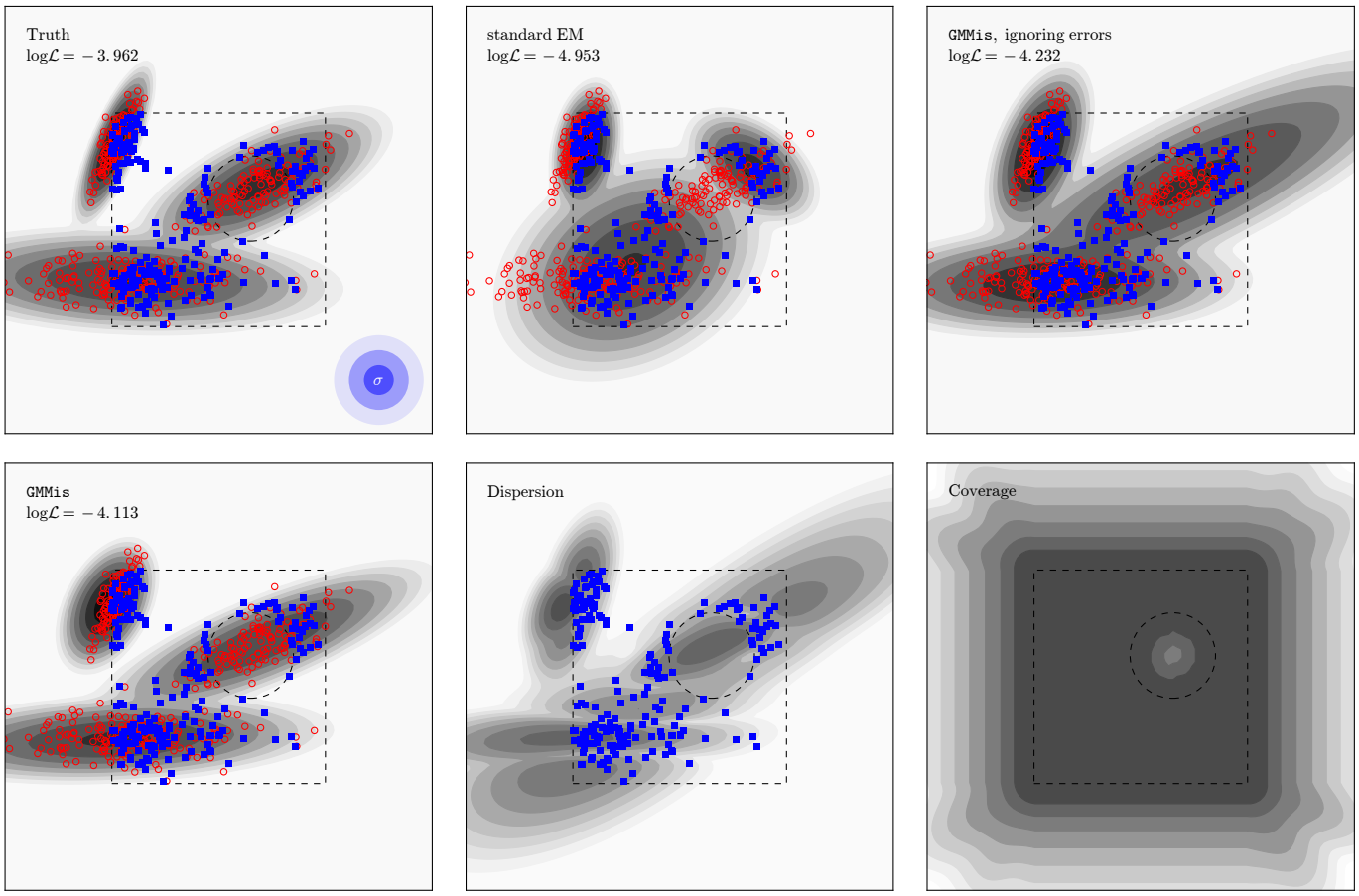

Figure 1: Test case for the EM algorithm with noisy and incomplete samples. *Top left*: True density distribution (contours in arcsinh stretch), a derived sample with $N = 400$ (red open circles, whose average log $\mathcal{L}$ under the respective models is given in the top-left corner of each panel), and the test sample (blue squares) after adding Gaussian noise (whose 1,2,3 σ contours are shown in the bottom-right corner) and rejecting all points outside of the box or inside the circle (dashed curves). *Top center*: Result of the standard EM algorithm (Equation 6). *Top right*: Result of the proposed EM algorithm `GMMis` (Equation 10), assuming noise-free samples. *Bottom left*: Result of `GMMis`, accounting the positional uncertainties of the sample (Equation 8). *Bottom center*: Standard deviation of the predicted $p(\mathbf{x})$ from 10 runs of `GMMis` as in the bottom-left panel. *Bottom right*: Estimated coverage (contours in log stretch) from 10 runs of `GMMis` as in the bottom-left panel (cf. Section 3.6 for details). Markers, if present, and completeness boundaries are identical in all plots.

$K = 50$ GMM components randomly in the $d = 3$ unit cube. Covariances are chosen such that the overlap between the components is not excessive; weights are drawn from a symmetric Dirichlet distribution with concentration parameter of unity. We impose a probabilistic completeness function $p(\Omega\,|\,\mathbf{x}) = 1 - x_1$, i.e. a linear ramp from fully observed to fully missing along one of the coordinate axes. The purpose of this setup is to allow all combinations of component weight α_k and completeness Ω. We draw N=10,000 samples from the model, apply Ω, and record the size of samples N_k drawn from each component k as well as the mean Ω_k experienced by those samples, so that we can compute the observed sample size $N_k^O = N_k\Omega_k$. No noise is added to the samples. An example cube is shown in Figure 3.

We then fit the test data with another GMM with the same $K = 50$, resulting in best-fit parameters $\tilde{\boldsymbol{\theta}}$, and repeat the process 10 times. As diagnostic, we directly compare the densities $\rho(\mathbf{x})$ by splitting the cube into 50^3 cells and counting the input samples that fall into the cell covering $\mathbf{x}$. We do the same for the predicted density $\tilde{\rho}(\mathbf{x})$ by drawing N samples from the fit. As we know the expectation value of Ω at the location of each cell, we can compute the fractional bias in the predicted density $(\tilde{\rho}(\mathbf{x}) - \rho(\mathbf{x}))/\rho(\mathbf{x})$ as a function of Ω (Figure 4). The standard EM algorithm provides a reliable estimate of the *observed* density, in other words: the bias is equal to Ω. The reason for positive bias for $\Omega > \frac{1}{2}$ lies in the normalization of the density estimator: as we drew the same number of samples N from the model as where given as input data, any underestimation of the density must be compensated elsewhere.

In the same test, `GMMis` shows a noticeably reduced sensitivity to Ω, but the resulting density estimate is still biased. This test demonstrates that there must be conditions under which the proposed algorithm fails. It is obvious that we cannot expect

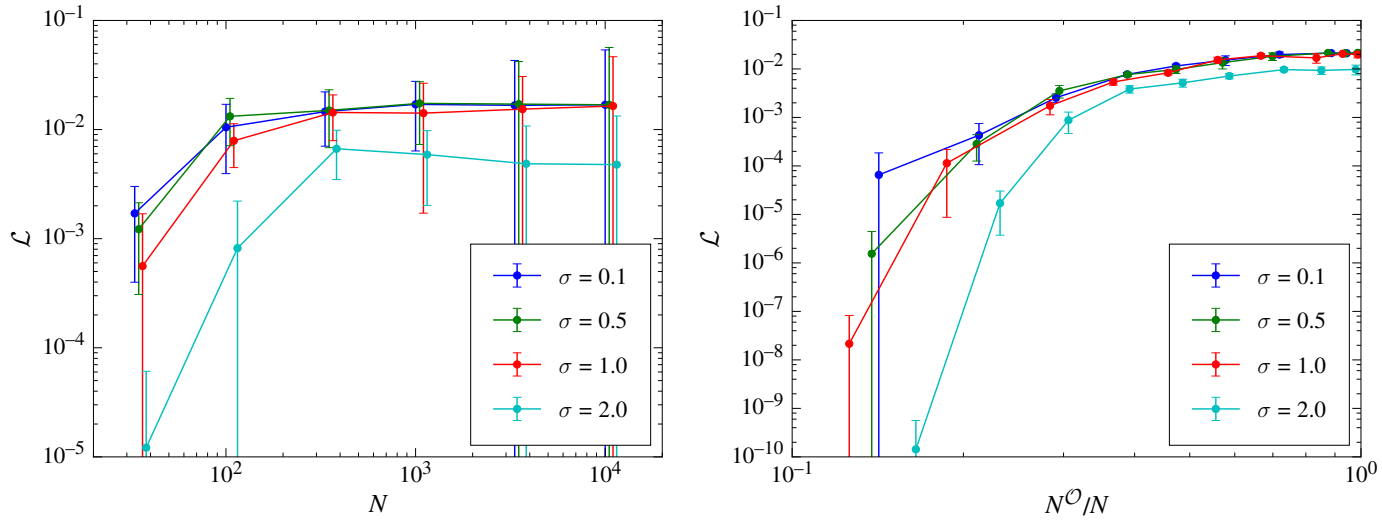

Figure 2: Reconstruction fidelity for the three clusters in Figure 1 with a box-shaped boundary of Ω as a function of sample size N (*left*) and observed sample fraction N^O/N (*right*). Added noise is isotropic bivariate normal and should be compared to the effective cluster widths of 1.45, 1.15, and 0.57. The observed fraction in the left panel is $N^O/N \approx 0.6$, the sample size in the right panel is held constant at $N = 1000$, while the observed fraction is varied by changing the size of the box. Errorbars denote the standard deviation of 50 runs.

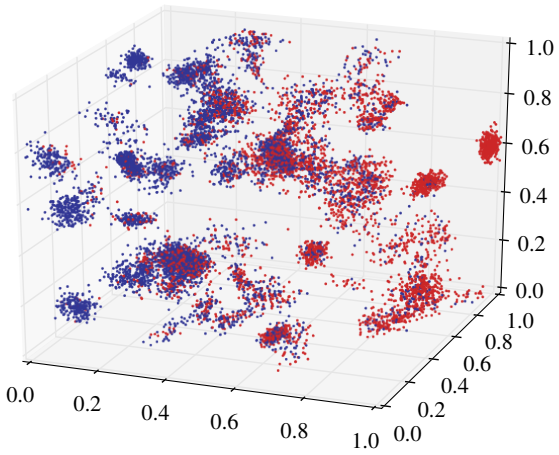

Figure 3: Example test data generated from $K = 50$ clusters in the $d = 3$ unit cube. The completeness Ω is probabilistic, decreasing linearly from unity (left side of the cube) to zero (right side). Observed samples are shown in blue, missing samples in red.

`GMMis`, or any other density estimator, to infer the properties or even existence of a cluster that is entirely unobserved, i.e. $N_k^O = 0$. Even for less extreme cases, Figure 4 shows that `GMMis` struggles with samples from regions with low Ω, overcompensating in regions with high Ω.

To determine limits of applicability, we evaluate how well the input samples from each component are described by the fit. We compute the association fraction η_k of the input sample from component k that falls within "1 σ" of any component of the fit, which, for $d > 1$, is more precisely expressed as $\{i : (\mathbf{x}_i - \tilde{\boldsymbol{\mu}}_k)^\top \tilde{\boldsymbol{\Sigma}}_k (\mathbf{x}_i - \tilde{\boldsymbol{\mu}}_k) \leq \chi^2_d(0.683) \text{ for any } k\}$, where χ^2_d is the quantile function of the chi-squared distribution with d degrees of freedom. For a component of the test data whose samples are perfectly fit (i.e. fit by the component from which they are generated), the association fraction should on average be $\eta_k = 68.3\%$. If η_k is higher, either the associated component of the fit is too extended or the test samples are associated with multiple components. If η_k is lower, the fit has effectively ignored some samples from input component k. In Figure 5 we plot η_k as a function of the effective weight N_k^O/N^O of component k given the observed data, while the size of the marker encodes the initial weight $\alpha_k = N_k/N$, and the color encodes Ω_k. It is apparent that components of the test data with large α_k or Ω_k are generally well-described by the fit. For $\Omega_k \approx 0$, the fit will miss a large fraction of the original sample irrespective of α_k, but there are also a few well-observed but low-α components that are largely being ignored by the fit. There is also an increased tendency of fitting multiple nearby input clusters with one larger component, which leads to artificially large η_k at low N_k^O/N^O.

Without formal proof, we seek a criterion to identify components that are too poorly observed to yield a reasonable fit. By performing the test described above with different values of N, K, component volumes, and Dirichlet concentration parameter, we found

$$\frac{N_k^O}{N^O} = \frac{N_k \Omega_k}{\sum_k N_k \Omega_k} \gtrapprox \frac{1}{K} \tag{18}$$

to perform well (shown as vertical dotted line in Figure 5). This qualitatively agrees with findings of e.g. Naim & Gildea (2012) that the best GMM fits with an EM algorithm are achieved when all components have approximately equal weights, in particular

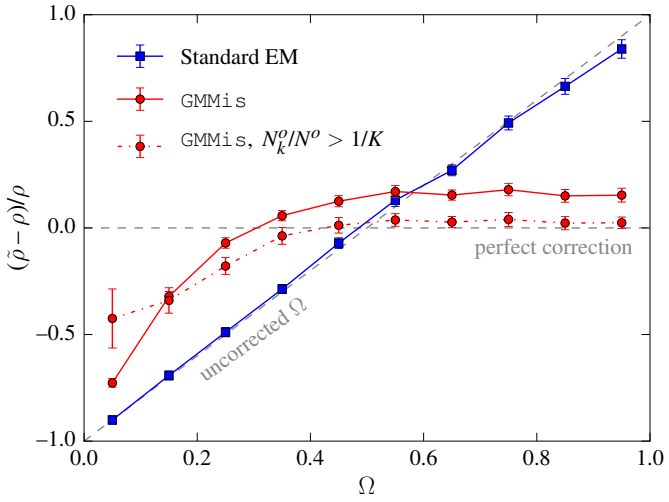

Figure 4: Relative bias of the density estimator as function of completeness Ω. The density is calculated by generating $N = 10,000$ samples from the fit and binning them into 50^3 cells within the unit cube: for the standard EM algorithm (blue) which does not correct for incomplete samples; for `GMMis` (solid red); for `GMMis` after removing all poorly observed components from the input data that do not obey Equation 18 (red dash-dotted).

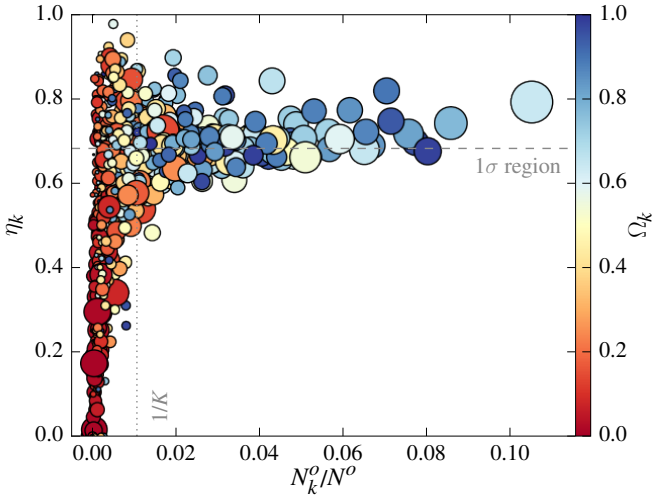

Figure 5: Associated fraction η_k of input samples to fit components as function of the effective weight in the observed data. Marker sizes denote weights α_k in the input data, colors refers to the average completeness Ω_k experienced by input components k. The horizontal dashed line shows the perfect outcome of 68.3% of the samples found within the "1σ region" of an output component; the vertical dashed line shows the criterion Equation 18 for likely unrecoverable components.

when they overlap. It also implies that `GMMis` has to successfully fit the observed distribution first to be able to generate meaningful imputation samples $\mathcal{M}$ that account and correct for Ω. If the first step is flawed, the second one will be, too.

This two-step picture is confirmed when we remove from the test data all components that would have violated Equation 18, in other words, the test data now only comprises clusters that remain salient despite Ω. In this case, the algorithm can detect all present clusters and correct for the sample incompleteness. Accordingly, the `GMMis` density estimates are now largely unbiased (dash-dotted red line in Figure 4). We emphasize that this shortcoming is not caused by an incorrect form of the likelihood, rather by the economy of the EM algorithm to converge to the nearest likelihood maximum, which favors the most prominent clusters in the observed sample. If, on the other hand, the parameters of all but one component were fixed at their true values and there were only one component left to fit, this component could experience incompleteness in excess of Equation 18 and still be fit with a fidelity commensurate to its number of samples N_k.

5. Application to X-ray data

In observational astronomy, truncated data occur frequently, caused e.g. by gaps between sensors or by proximity to bright objects that render a portion of the observation useless. As a milder form of incomplete data, long-running observing campaigns routinely encounter variations in how well the sky can be observed, for instance when the transparency of the atmosphere or the brightness of the moon changes. As a consequence, astronomical surveys exhibit complicated completeness functions for the density of observed samples and derived data products (e.g. Leistedt et al., 2016).

For this work, we analyze the distribution of X-ray photons of the nearby ($D \sim 16$ Mpc) galaxy NGC 4636, observed with the Advanced CCD Imaging Spectrometer (ACIS) aboard the *Chandra* telescope. These data were retrieved from the *Chandra* public archive, and consist of two individual 75 ks pointings (Observation Identification Numbers 3926 and 4415). Basic data processing was carried out following the procedure described in Goulding et al. (2016). Briefly, we used the *Chandra* X-ray Center pipeline software packages available in CIAO v4.7 to apply the latest detector calibration files, and remove the standard pixel randomization, streak events, bad pixels, and cosmic rays. Photon catalogs (referred to as "events files") were screened using a typical grade set (grade = 0, 2, 3, 4, 6), and cleaned of 3σ background flares. Finally, aspect histograms were constructed and convolved with the ACIS-I chip map, using the CIAO tool `mkexpmap`, to generate the observation specific exposure time maps.

In the top-left panel of Figure 6 we show a histogram of ≈ 150,000 photons in the energy range $E \sim 0.5 - 2$ keV, covering an area with a side-length of about 0.3 degrees. Two features of the observation are obvious. First, there are small gaps between the four CCDs of ACIS-I, where the ability to record photons is strongly reduced. In detail, ACIS additionally suffers from minor and well-known sensitivity degradations in different parts of the CCD (top-right panel of Figure 6). Second, besides the galaxy, there is an essentially uniform particle background, as well as additional smaller objects ("point sources"). These point sources are a mixture of X-ray binary systems that

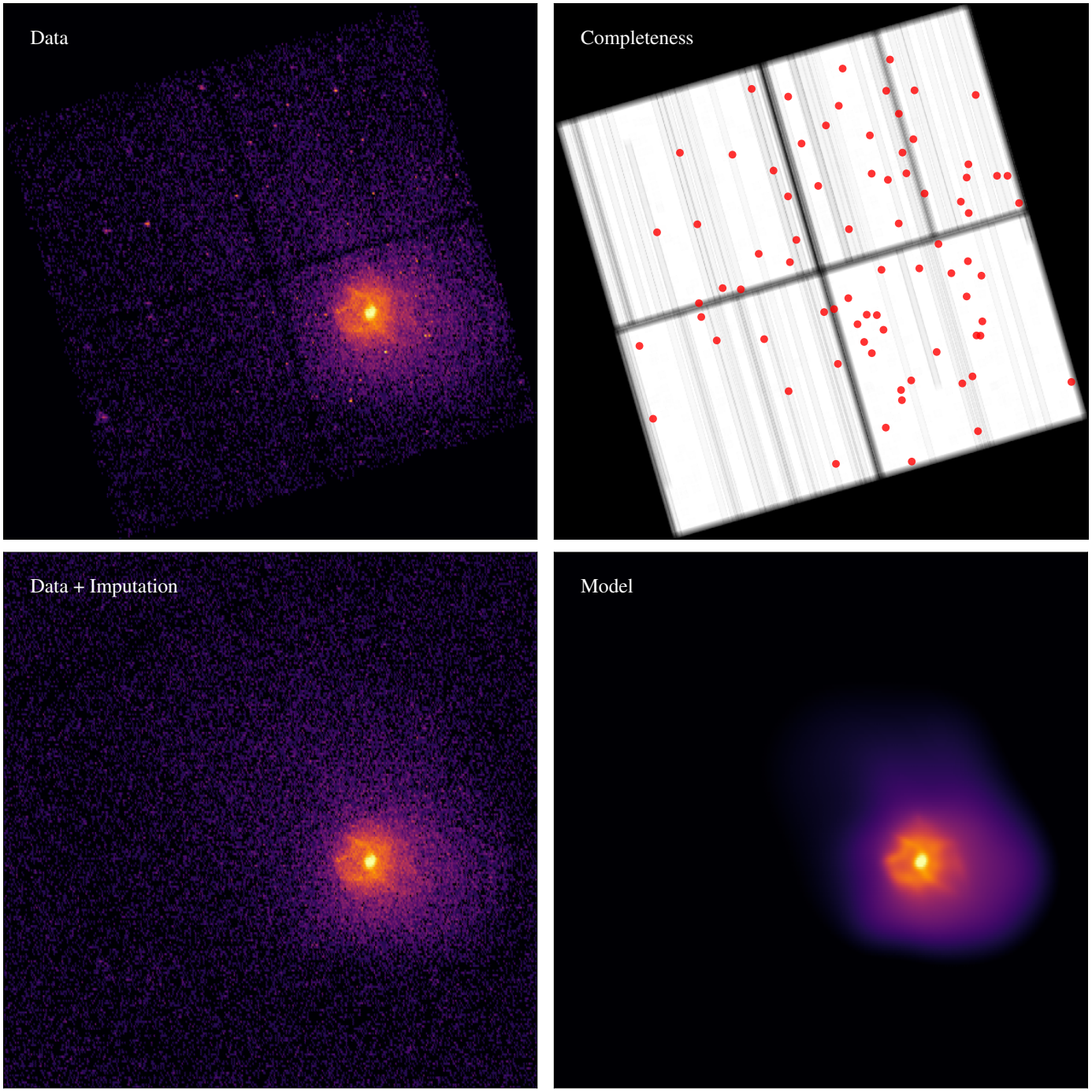

Figure 6: Application to X-ray data. *Top left*: Histogram of the locations of photons in the energy range 0.5–2 keV for an observation of the galaxy NGC 4636 with the ACIS-I instrument of the *Chandra* X-ray telescope. *Top right*: Completeness $\Omega(\mathbf{x})$ for ACIS-I, determined by the location of its four CCDs and detector sensitivity variations; point source masks (red circles, sizes true to scale), where we reject data and explicitly set $\Omega = 0$, have been added for the purpose of this analysis. *Bottom left*: ACIS-I data augmented with the imputation sample drawn from the final models of the GMM and the background. *Bottom right*: Final GMM with $K = 60$ of the extended emission of the galaxy, after rejecting point sources and removing the background. All panels are shown in logarithmic stretch.

are intrinsic to NGC 4636 and distant, rapidly growing supermassive black holes unrelated to the target galaxy. We mask the point sources with small circular apertures (shown as red dots), a step that is commonly done in the analysis of X-ray data.

As a further complication, the photon positions are not known exactly as they have been convolved with the instrument Point-

spread function (PSF), which for this ACIS-I has a shape that is very well approximated by a circular Gaussian[4] with a width that varies from 0.4 arcsec in the inner region of ACIS-I to 15 arcsec at the perimeter.

Our new method is ideally suited to directly analyze the photon event files. We can account for chip gaps, field edges, sensitivity variations, and point-source masks with the basic `GMMis` algorithm from Section 2.3. By recognizing that convolution with the PSF is formally identical to additive measurement noise, we can employ the deconvolution method from Section 2.2 to build a generative model of the underlying, noise-free distribution of X-ray photons, while simultaneously fitting for the X-ray background as described in Section 3.4. In contrast, a more traditional image analysis typically entails smoothing, which does not correctly account for any form of sample incompleteness, and a single deconvolution step, which does not incorporate the spatial variation of the PSF width.

The bottom-left panel of Figure 6 demonstrates the principle of operations. By drawing samples from the current state of the model, which comprised the GMM and the uniform background, convolving them with the spatially varying PSF, and selecting them according to Ω, we get a sample to augment the observed data. Combining this imputation sample and the point-source masked data, we get a representation of the internal state of the model, in other words: its estimate how the data would look like if $\Omega = 1$. In each iteration these augmented data enter Equation 10 to determine the best-fit model of the extended emission of the galaxy without point sources (bottom-right panel).

We initialize the GMM with $K = 60$ components with means distributed according to a bivariate Gaussian, whose width s was determined by fitting the galaxy with $K = 1$ first. Because the scene exhibits features of different scales, we set the component covariances to $\mathbf{\Sigma}_k = 4^{-l} s^2\, \mathbf{I}$ with $l = 0, \ldots, 5$, and 10 components at each level l. This tailored initialization is necessary despite the GMM's ability to adjust to arbitrary configurations because the rate of convergence is very slow for the weakly expressed features we are particularly interested in. The background amplitude ν was allowed to vary between 0.2 and 0.5, with $\nu = 0.396$ being the best-fit value, in other words about 40% of the photons over the unobscured region shown in Figure 6 originate from the background.

The GMM is capable of faithfully describing the bulk and finer features in the data: a bright, apparently bimodal central region, most likely arising due to the presence of an accreting supermassive black hole; an extended halo of low-intensity emission from diffuse, several thousand degree hot gas with a noticeable skewness towards the lower right corner; and the location and intensity of several shock fronts caused by buoyantly rising pockets of plasma that were likely inflated during previous outbursts of the central supermassive black hole. However, because of the complexity of the model with $K = 60$, it is not guaranteed that particular features, e.g. shock fronts, are fit by a single component. This association could be made more clearly if the analysis operated on a three-dimensional feature space of photon positions and energies, a study we leave for the future.

Because this is a demonstration of the capabilities of the method, we have not performed e.g. cross-validation tests to determine the optimal K. The model is the result of a single run with a number of components that appeared visually reasonable to capture the key features of the data. Its χ^2 per degree of freedom over an area where the galaxy dominates the emission is at least 1.34,[5] indicating that a larger number of components would be necessary to capture all significant features.

6. Summary and conclusions

We describe an extended EM algorithm to perform density estimation with Gaussian mixture models in situations where the data exhibits a known incompleteness Ω. The type of incompleteness may be described by a simple binary decision boundary, a case that is usually denoted as "truncated data", or by an arbitrary probabilistic function $\Omega(\mathbf{x})$, as long as the mechanism that causes the incompleteness is independent of the density (*missing at random*).

The key difference of the method described here to the situation that is often—and somewhat ambiguously—called "missing data" is that the latter refers to data, for which some features of any data sample may be absent. In contrast, we deal with entire samples being potentially absent, caused by the systematic limitation to observe the entire feature space or all of its relevant subdomains.

Our solution is based on drawing imputations samples from the current state of the GMM, and to recompute the model parameters in the M-step using both observed and missing samples. This technique is applicable to any generative model that is fit with an EM algorithm. Its advantage is the flexibility to efficiently adjust to any incompleteness $\Omega(\mathbf{x})$ as one avoids the analytic integration of the predicted density over the incomplete subdomains. Instead, we draw test samples from the GMM, retain those that would not have been observed under Ω, and obtain non-zero contributions to the moments of those components that extend into incompletely observed subdomains. If the model is accurate, adding those moments to the ones obtained from the observed samples results in parameter estimates consistent with those for completely observed data.

We detail practical adjustments of the algorithm, regarding its initialization, split-and-merge operations, and simultaneously fitting for a uniform background. We also recommend averaging GMMs from independent runs to smooth out the dependence of the EM algorithm on the starting position, and describe how the uncertainty of the estimators and coverage of the features space can be estimated.

In simplified tests we demonstrate that the algorithm

1. recovers an estimate of the underlying density in presence of complex incompleteness functions,

[4] See the *Chandra* Proposers' Observatory Guide, `http://cxc.harvard.edu/proposer/POG/`

[5] For the estimate of the degrees of freedom we assumed that no parameters are learned from the data, yielding an upper bound on the dof. If all parameters were linearly independent, which is not an appropriate assumption for GMMs, the dof would be reduced by 3%.

2. correctly accounts for incompleteness and additive noise if the imputation samples describe the *noisy* unobserved data,

3. can only partially correct for incompleteness if the too many of the original samples have not been observed.

The last finding is central to the applicability of the method. Constraining complex GMMs with finite amounts of samples becomes even more challenging with non-neglibible incompleteness. Correcting for the latter requires being able to perform the former reasonably well, otherwise the imputation samples do not describe the true unobserved samples. In absence of an analytical estimate of the fidelity of GMMs from the EM algorithm, we provide a best-effort estimate for the limits of the algorithm in Equation 18.

We demonstrate the usefulness of the algorithm with an example from observational astronomy, where the incompleteness stems from gaps between the chips of the ACIS instrument aboard the NASA X-ray telescope *Chandra*. We directly estimate the extended emission of the galaxy NGC 4636 from the location of photon hits, while accounting for the window-frame configuration of the detector, the spatially varying point-spread function, and an uniform X-ray background.

The presented method provides an efficient and flexible tool to estimate the density of a process that is affected by moderate levels of incompleteness of the MAR type. As such situations may arise in many areas of the physical and social sciences, we believe this contribution to be of general use and have therefore made our PYTHON implementation available at `https://github.com/pmelchior/pyGMMis`.

Appendix A. Missingness for density estimation

To understand what form the likelihood assumes when some samples are not observed, we need to determine how observed and missing samples are related. For this purpose Rubin (1976) introduced the missingness mechanism R that determines which part of the complete data $\mathbf{Y}$ is observed ($\mathbf{Y}_o$) or missing ($\mathbf{Y}_m$). The relation between R and $\mathbf{Y}_o$ or $\mathbf{Y}_m$ gives rise to three distinct types of missingness:

$$p(R\,|\,\mathbf{Y}) = \begin{cases} p(R) & \text{missing completely at random (MCAR)} \\ p(R\,|\,\mathbf{Y}_o) & \text{missing at random (MAR)} \\ p(R\,|\,\mathbf{Y}_o, \mathbf{Y}_m) & \text{missing not at random (MNAR)} \end{cases}$$

Under MCAR, the missingness mechanism does not depend on the data at all; in turn, the data do not reveal properties of R. The key distinction between MAR and MNAR is whether R depends only on observed or also on missing features.

For the problem of density estimation with incomplete samples $\mathbf{x}$, it is not immediately obvious what $\mathbf{Y}_o$ and $\mathbf{Y}_m$ correspond to. We take guidance from the close relation between density estimation and function approximation by positive linear operators (e.g. Ciesielsky, 1991). We therefore take $\mathbf{X}$ to be the entire feature space $\mathbb{R}^d$ and $\mathbf{Y} = \mathbb{R}$ the co-domain of a scalar function $p : \mathbf{X} \to \mathbf{Y}$, namely the PDF $p(\mathbf{x})$. The data then span $(\mathbf{X}, \mathbf{Y}) = \mathbb{R}^{d+1}$, and R determines at what locations $\mathbf{x}$ a value $y \in \mathbf{Y}$ is recorded.

In Section 2.3, we introduced the completeness function $\Omega(\cdot)$, which is equivalent to $p(R\,|\,\cdot)$. Only a spatially uniform completeness function fulfills the MCAR condition. If Ω only depends on $\mathbf{x}$, the MAR condition applies because $\mathbf{X}$ is by construction completely observed (only values of $\mathbf{Y}$ may be missing). Technically, MAR still holds if Ω depends on $\mathbf{x}$ and the density $p(\mathbf{x}')$ at some other observed position $\mathbf{x}' \neq \mathbf{x}$, for instance when the observed samples "shadow" some others. For the sake of brevity, we have not listed this case in Equation 9. Only if samples are missing because of their own value of $p(\mathbf{x})$, or because of their relation to other missing values $p(\mathbf{x}')$, we have MNAR. This can happen e.g. when an experimental device is locally invalidated by saturation or if samples are only recorded if their local abundance exceeds a certain threshold.

References

References

Biernacki C., Celeux G., Govaert G., 2003, Comput. Stat. Data Anal., 41, 561
Blömer J., Bujna K., 2013, preprint, (arXiv:1312.5946)
Bovy J., Hogg D. W., Roweis S. T., 2011, Annals of Applied Statistics, 5, 1657
Breiman L., 1996, Machine Learning, 24, 49
Cadez I. V., Smyth P., McLachlan G. J., McLaren C. E., 2002, Mach. Learn., 47, 7
Ciesielsky Z., 1991, Probability And Mathematic Statistics, 12, 1
Dempster A. P., Laird N. M., Rubin D. B., 1977, Journal of the Royal Statistical Society. Series B (Methodological), 39, 1
Frühwirth-Schnatter S., 2006, Finite Mixture and Markov Switching Models. Springer Series in Statistics, Springer New York, http://www.springer.com/us/book/9780387329093
Goulding A. D., et al., 2016, ApJ, 826, 167
Lee G., Scott C., 2012, Comput. Stat. Data Anal., 56, 2816
Leistedt B., et al., 2016, ApJS, 226, 24
McLachlan G. J., Jones P. N., 1988, Biometrics, 44, 571
McLachlan G., Peel D., 2000, Finite Mixture Models, Wiley Series in Probability and Statistics. John Wiley & Sons, New York, https://books.google.com/books?id=YXqflwEACAAJ
Naim I., Gildea D., 2012, preprint, (arXiv:1206.6427)
Rubin D. B., 1976, Biometrika, 63, 581
Rubin D., 1987, Multiple Imputation for Nonresponse in Surveys, Wiley Series in Probability and Statistics. Wiley Series in Probability and Statistics, Wiley, https://books.google.com/books?id=0KruAAAAMAAJ
Schafer J. L., Graham J. W., 2002, Psychological Methods, 7, 147
Smyth P., Wolpert D., 1999, Machine Learning, 36, 59
Ueda N., Nakano R., Ghahramani Z., Hinton G. E., 2000, Journal of VLSI signal processing systems for signal, image and video technology, 26, 133
Wolpert D. H., 1992, Neural Netw., 5, 241
Wolynetz M. S., 1979, Journal of the Royal Statistical Society. Series C (Applied Statistics), 28, 195
Wu C. F. J., 1983, The Annals of Statistics, 11, 95
Zhang Z., Chen C., Sun J., Chan K. L., 2003, Pattern Recognition, 36, 1973